Sci

MDPI

Article

Correlation of AFM-Derived Surface Topography with Nitrogen Adsorption Measurements for the Surface Characterization of a Au/γ-Al_2O_3 Catalyst

Dimitris-Phoebus Tsaousoglou, Charikleia Prochaska, Sotirios Sotiropoulos and Dimitrios Gavril *

Laboratory of Physical Chemistry, Department of Chemistry, Aristotle University of Thessaloniki, GR-54124 Thessaloniki, Greece; dtsaousa@chem.auth.gr (D.-P.T.); prohaska@chem.auth.gr (C.P.); eczss@chem.auth.gr (S.S.)
* Correspondence: dgavriil@chem.auth.gr

Abstract

The structural and surface characteristics of supported heterogeneous catalysts were investigated using a combination of nitrogen adsorption-desorption porosimetry and Atomic Force Microscopy (AFM). A Au/γ-Al_2O_3 catalyst was characterized in terms of specific surface area, pore size distribution, surface morphology and roughness. Nitrogen adsorption measurements revealed type IV isotherms, confirming their mesoporous nature. The Au/γ-Al_2O_3 catalyst exhibited a BET surface area of 266 m^2 g^{-1} and a dominant mesopore size distribution centred approximately within the 9–13 nm range. AFM imaging was employed to investigate the nanoscale surface topography and revealed a heterogeneous surface. Quantitative image analysis was further performed using threshold segmentation and grain analysis to identify nanoscale topographical depressions and surface features. A total of 2539 surface features were detected, corresponding to a planar surface fraction of 6.71%. Characteristic lateral dimensions of surface features derived from the image analysis were found to be in the range of approximately 9–12 nm, indicating that these can be correlated with pores since they bear similar dimensions to the latter (as estimated by porosimetry). Statistical validation using Student's t-test demonstrated good agreement between local measurements obtained from representative scan lines and the overall image-based analysis. Surface roughness measurements yielded average roughness (*R*a) and root mean square roughness (*R*q) values of 2.06 ± 1.90 nm and 3.42 ± 1.91 nm, respectively, indicating a moderately rough nanostructured surface. The characteristic dimensions of the AFM-derived surface features were found to be consistent with the mesopore size range determined independently by nitrogen adsorption but they do not directly represent internal pores. AFM probes only the external surface morphology and does not directly characterise the internal pore network. The combined approach demonstrates that AFM image analysis can provide valuable complementary information on catalyst surface morphology, roughness and nanoscale textural features alongside conventional gas adsorption techniques.

Keywords: Au catalysis; γ-Al_2O_3; Atomic Force Microscopy; nitrogen porosimetry; surface topography

Check for updates

Academic Editor: Kang Sun

Received: 17 September 2026
Revised: 19 October 2026
Accepted: 23 October 2026
Published: 4 November 2026

Copyright: © 2026 by the authors. Licensee MDPI, Basel, Switzerland. This article is an open access article distributed under the terms and conditions of the Creative Commons Attribution (CC BY) license.

1. Introduction

Supported heterogeneous catalysts are among the most important materials in modern catalysis and are extensively employed in environmental remediation, petrochemical processing, hydrogen production, fuel synthesis, and energy conversion technologies [1–5].

These materials consist of an active phase, typically transition or noble metal nanoparticles, dispersed on a high-surface-area support. The support not only provides mechanical and thermal stability but also promotes the dispersion of the active phase, thereby increasing the density of accessible catalytic sites and enhancing catalytic performance [1–4]. High metal dispersion further mitigates nanoparticle sintering and catalyst deactivation, phenomena that often occur under severe reaction conditions and lead to loss of catalytic activity [4].

Among the various support materials available, γ-Al_2O_3 remains one of the most widely used owing to its high specific surface area, favourable metal-support interactions, chemical stability, and well-developed porous structure [6–11]. In addition to its textural properties, γ-Al_2O_3 exhibits a complex defective crystal structure containing vacant spinel sites and a combination of tetrahedral and octahedral aluminium environments, which significantly influence its surface chemistry and catalytic behaviour [8–11]. The dispersion of supported nanoparticles, the accessibility of reactants to active sites, and mass transport phenomena are all strongly affected by the support's surface area, porosity, and surface morphology. Consequently, detailed characterization of both the internal porous network and the external surface structure is essential for understanding catalyst performance and stability.

Nitrogen adsorption-desorption porosimetry is one of the most employed techniques for characterizing porous catalytic materials [12–15]. By measuring the adsorption of nitrogen at cryogenic temperatures, information can be obtained regarding the specific surface area, pore volume, pore size distribution, and pore network characteristics of porous solids. The Brunauer-Emmett-Teller (BET) theory remains the standard approach for determining specific surface area, while pore size distributions can be evaluated using methods such as Barrett-Joyner-Halenda (BJH) and non-local density functional theory (NLDFT) [12,13]. Nitrogen adsorption is particularly valuable for mesoporous catalyst supports because it provides statistically representative information from the entire sample volume. However, the technique provides only indirect information regarding local surface morphology and cannot directly visualize nanoscale surface features or surface heterogeneities [14,15].

Surface topography is increasingly recognised as a critical parameter governing catalyst performance. Nanoscale variations in surface morphology influence particle nucleation and growth during catalyst preparation, affect the distribution and anchoring of active metal nanoparticles, and may alter local reaction environments at catalytic interfaces [16–18]. Recent studies have further demonstrated that catalyst surfaces evolve dynamically during operation through mechanisms such as restructuring, dissolution-redeposition, agglomeration, and defect generation, processes that are highly dependent on local surface geometry and morphology [19]. For these reasons, the direct investigation of catalyst surface topography has become increasingly important for establishing structure-property relationships in heterogeneous catalysis.

Atomic Force Microscopy (AFM) represents one of the most powerful techniques available for nanoscale surface characterization [16–18]. Unlike optical or electron microscopy, AFM operates by monitoring the interaction forces between a sharp probe and a sample surface while scanning the specimen in a raster pattern. This approach provides three-dimensional topographical information with nanometre-scale lateral resolution and sub-nanometre vertical resolution. In addition to imaging, AFM enables quantitative determination of surface roughness parameters and nanoscale morphological features under ambient conditions. Nevertheless, interpretation of AFM images requires careful consideration of limitations such as tip convolution effects, contamination layers, and the fact that only the external surface morphology is probed directly [16–18].

Nitrogen adsorption provides statistically representative information on the internal porous architecture, whereas AFM directly visualizes surface topography and roughness.

Consequently, the complementary use of these techniques offers an opportunity to obtain a more comprehensive understanding of catalyst structure and investigate whether surface morphological features observed by AFM reflect the textural characteristics determined independently by gas adsorption methods.

In the present work, a 5 wt.% Au/γ-Al_2O_3 catalyst was investigated using nitrogen adsorption-desorption porosimetry and Atomic Force Microscopy. AFM analysis revealed a heterogeneous nanostructured surface consisting of protrusions compatible with Au nanoparticles and their aggregates and nanoscale topographical depressions distributed across the alumina support surface. The characteristic dimensions of the AFM-derived surface features were found to be consistent with the mesopore size range obtained from nitrogen adsorption, suggesting that nanoscale surface features identified by AFM possess dimensions comparable to the characteristic mesopore size range determined independently by nitrogen adsorption.

2. Materials and Methods

2.1. Catalyst Materials

The present study focused on the structural characterization of a nanostructured Au/γ-Al_2O_3 supported catalyst. The catalyst, with a nominal gold loading of 5 wt.%, was prepared by homogeneous deposition-precipitation, a synthesis method known to produce highly dispersed gold nanoparticles with typical particle sizes in the range of 3–5 nm [20–22]. An aqueous $HAuCl_4$ solution was mixed with γ-Al_2O_3 support material in the presence of excess urea at an initial pH of approximately 4. The suspension was vigorously stirred and heated at 70–75 °C to promote the controlled decomposition of urea, leading to a gradual increase in pH and homogeneous precipitation of gold species onto the alumina surface. After reaching pH 8, the precipitate was filtered, washed repeatedly to remove chloride ions, and dried under ambient conditions. Subsequently, the catalyst was dried in air at 80 °C for at least 16 h and calcined under oxygen flow at 300 °C for 2 h using a heating rate of 5 °C min^{-1}.

The catalyst synthesis procedure and its physicochemical characterization have been described previously [20–26]. The actual gold loading determined by atomic absorption spectroscopy (AAS) was 5.1 ± 0.3 wt.%, while the mean gold particle diameter was measured as 4.2 nm by X-ray diffraction (XRD) and 3.6 ± 1.4 nm by high-resolution transmission electron microscopy (HRTEM) [20–25]. These analyses confirmed the presence of highly dispersed metallic gold nanoparticles on the γ-Al_2O_3 support. Although XRD, HRTEM and XPS measurements predominantly indicated metallic gold, the presence of trace amounts of oxidized gold species could not be completely excluded [20–25].

2.2. Nitrogen Adsorption–Desorption Porosimetry

The textural properties of the catalyst were investigated by nitrogen adsorption-desorption measurements at −196 °C (77 K) using an Autosorb-1 MP Automatic Volumetric Sorption Analyzer (Quantachrome Instruments, Boynton Beach, FL, USA). Prior to analysis, the samples were degassed under vacuum (5×10^{-9} Torr) at 150 °C for 16 h in order to remove physisorbed contaminants and moisture from the catalyst surface.

The specific surface area was determined using the Brunauer–Emmett–Teller (BET) multi-point method [12]. Mesopore size distributions and mean pore diameters were calculated from the adsorption branch of the nitrogen isotherm using the Barrett–Joyner–Halenda (BJH) method [27]. Micropore volume and micropore surface area were estimated by means of the t-plot method.

To complement the classical pore-size analysis, pore-size distributions were additionally evaluated using the non-local density functional theory (NLDFT) approach [14,28].

NLDFT determines pore-size distributions through the fitting of experimental adsorption isotherms with theoretical adsorption kernels generated for ideal pore geometries. The corresponding adsorption integral equation is solved using regularization procedures to obtain the most probable pore-size distribution [14].

The BJH method was selected because of its extensive application in the characterization of mesoporous materials. This method assumes cylindrical pore geometry and combines multilayer adsorption and capillary condensation phenomena through the Kelvin equation to calculate pore-size distributions from adsorption–desorption isotherms [14,27,28].

2.3. Atomic Force Microscopy (AFM)

Surface morphology and roughness were investigated using an NT-MDT SOLVER-PRO Atomic Force Microscope (NT-MDT, Moscow, Russia). All measurements were carried out under ambient atmospheric conditions at room temperature (approximately 20 °C). The microscope was mounted on a vibration-isolation system to minimize environmental perturbations during image acquisition.

AFM measurements were performed in contact mode using a silicon cantilever (CSG30 Series, NT-MDT, Moscow, Russia) with a nominal resonance frequency in the range of 47–90 kHz, a nominal force constant of approximately 0.6 N m^{-1} (manufacturer-specified range: 0.24–1.7 N m^{-1}), and a tip radius of approximately 10 nm. The cantilever dimensions were 185–195 μm in length, 25–35 μm in width, and 0.5–1.5 μm in thickness. Samples were mounted on polycrystalline substrates using double-sided adhesive tape.

Scanning was carried out at 0.3 Hz with image acquisition at a resolution of 256 × 256 pixels. Sample tilt correction and noise filtering were applied where necessary using the NoVA software package (version 1.1.0.1912). A representative surface area of 3 μm × 3 μm with a vertical range of 40 nm was initially scanned to evaluate the overall topography of the catalyst surface. A selected region was subsequently imaged at higher magnification over an area of 600 × 700 nm^2 with a vertical range of approximately 4 nm. Quantitative grain analysis and calculation of the planar mask fraction were performed using the 3 × 3 μm^2 image, whereas the 600 × 700 nm^2 image was used only for higher-magnification visualization.

The acquired AFM micrographs revealed a heterogeneous nanostructured surface consisting of protrusions compatible with Au nanoparticles and their aggregates and nanoscale depressions distributed across the γ-Al_2O_3 support.

2.4. AFM Image Analysis and Surface Feature Quantification

Quantitative image analysis was performed using the open-source software package Gwyddion (version 2.61). The “Invert Height” and “Grain Analysis” functions were applied to processed AFM topographic images to identify and quantify nanoscale surface depressions. Similar image-processing methodologies have been successfully employed for the quantitative analysis of nanoscale surface heterogeneity and nanoporous materials [29,30]. Sample-tilt correction, image levelling or flattening, removal of faulty scan lines where necessary, and noise filtering were performed before quantitative analysis using the NoVA image-analysis software package (version 1.1.0.1912). The processed topographic data were subsequently analysed in Gwyddion. The height data were inverted, and threshold segmentation was applied interactively by adjusting the threshold until individual low-lying surface regions were visually distinguishable from the surrounding topography without obvious merging of adjacent regions.

The projected area was defined as the two-dimensional image-plane area occupied by each retained threshold-defined component, and the planar mask fraction was calculated as the cumulative projected area of all retained components divided by the total scanned area.

Maximum and minimum Feret diameters were used to describe the longest and shortest lateral caliper dimensions of the segmented components, respectively. Because threshold selection was visually guided, the resulting grain-analysis parameters were treated as operator-dependent, semi-quantitative descriptors of the segmented surface topography rather than as direct measurements of internal pore geometry.

The effective tip shape was estimated by blind tip reconstruction (Villarrubia algorithm, Gwyddion), and images were corrected by surface reconstruction before grain analysis. The identified features were characterized in terms of projected area, projected boundary length, maximum and minimum Feret diameters, and total feature count. The Feret diameter (dF) was defined as the distance between two parallel tangents measured at a specified orientation [29,30]. The maximum and minimum Feret diameters were used to describe the lateral dimensions of the segmented surface depressions.

To evaluate the representativeness of the image-analysis results, six independent line profiles were extracted from the analysed AFM image, comprising three horizontal and three vertical scan lines. Surface depressions identified along these profiles were manually measured and compared with the results obtained from the global grain analysis. Statistical evaluation was performed using Student's *t*-distribution with eighteen measurements in each direction and a confidence level of 99%. This procedure was employed to assess the consistency between local measurements and the overall image-based analysis. The reported grain-analysis and roughness parameters were therefore derived from this representative dataset and should not be interpreted as statistical averages obtained from multiple independent scan locations, samples, or batches. To evaluate the consistency of the grain-analysis procedure, selected segmented surface depressions identified in the processed AFM image were independently measured. Eighteen measurements were collected for each parameter investigated. A Student's *t*-test was subsequently applied with 17 degrees of freedom at a 99% confidence level to compare the manually measured dimensions with the corresponding grain-analysis results obtained from the entire image. Because all measurements originated from the same AFM image, the analysis was used only as an internal consistency check between manual and software-assisted measurements. It was not used to establish spatial representativeness, measurement repeatability, specimen-level variability, or batch-to-batch reproducibility.

2.5. Surface Roughness Calculation

Surface roughness parameters were calculated directly from the AFM topographic maps using Gwyddion software. The arithmetic average roughness (*R*a) and the root mean square roughness (*R*q) were selected as the principal descriptors of surface morphology, following established AFM surface-characterization methodologies [31].

*R*a represents the average absolute deviation of surface heights from the mean plane, whereas *R*q corresponds to the root mean square deviation and is therefore more sensitive to large height fluctuations [31]. These parameters were employed to quantitatively characterize the nanoscale roughness and topographical heterogeneity of the Au/γ-Al_2O_3 catalyst surface.

The combined methodology adopted in this study enabled the correlation of textural properties obtained from nitrogen adsorption–desorption measurements with nanoscale surface morphology and roughness derived from AFM topographical analysis [31].

3. Results

3.1. Textural Characterization of the Au/γ-Al_2O_3 Catalyst

Nitrogen Adsorption–Desorption Analysis

The nitrogen adsorption–desorption isotherm of the 5 wt.% Au/γ-Al_2O_3 catalyst is shown in Figure 1. The adsorption behaviour corresponds to a Type IV isotherm according to the IUPAC classification, confirming the mesoporous nature of the material. A pronounced hysteresis loop was observed at high relative pressures, indicating the occurrence of capillary condensation within the mesoporous network. The hysteresis profile resembles the H3 type, commonly associated with slit-shaped pores or aggregates of plate-like particles.

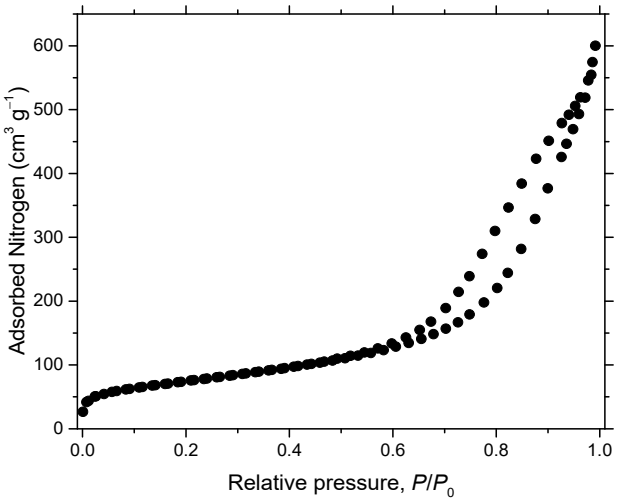


Figure 1. Nitrogen adsorption-desorption isotherm of the 5 wt.% Au/γ-Al_2O_3 catalyst measured at 77 K. The Type IV isotherm and hysteresis loop indicate the presence of a mesoporous structure.

The principal textural properties obtained from nitrogen adsorption measurements are summarized in Table 1. The catalyst exhibited a BET specific surface area of 266 m^2 g^{-1} and a total pore volume of 0.928 cm^3 g^{-1}. The micropore contribution was negligible, with a micropore volume of 0.003 cm^3 g^{-1} and a micropore surface area of 11 m^2 g^{-1}, indicating that the catalyst texture is dominated by mesoporosity.

Table 1. Textural properties of the Au/γ-Al_2O_3 catalyst.

Property	Au/γ-Al_2O_3
BET surface area (m^2 g^{-1})	266
Total pore volume (cm^3 g^{-1})	0.928
Micropore volume (cm^3 g^{-1})	0.003
Micropore surface area (m^2 g^{-1})	11
External surface area (m^2 g^{-1})	255

The mesopore size distribution obtained from the adsorption branch of the isotherm (BJH analysis) is presented in Figure 2. The distribution extends approximately from 10 to 1000 Å, with a maximum centred at approximately 130 Å (13 nm). Analysis of the desorption branch yielded a corresponding maximum near 90 Å (9 nm), indicating that the dominant mesostructural features are located in the 9–13 nm range. These results confirm the mesoporous character of the catalyst. The pore-size maximum was approximately 13 nm by BJH analysis of the adsorption branch, 9 nm by BJH analysis of the desorption branch, and 7.5 nm by NLDFT. The differences reflect the use of distinct calculation models and, for BJH, the different physical pathways represented by the adsorption and desorption branches.

Accordingly, the three values are reported separately and are not averaged. NLDFT is treated as the preferred model-based estimate, while the BJH adsorption result is used as the principal classical-method comparison.

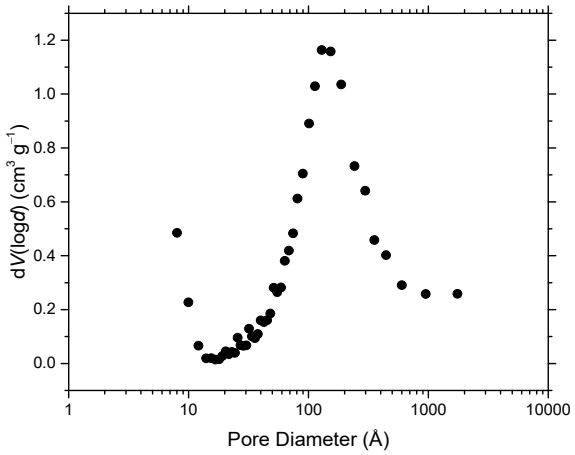


Figure 2. BJH pore size distribution obtained from the adsorption branch of the nitrogen isotherm for the Au/γ-Al_2O_3 catalyst. The distribution is centred within the mesoporous range with a maximum at approximately 13 nm.

Application of the NLDFT model provided a similar description of the catalyst texture, as in Figure 3. The calculated distribution ranged from approximately 40 to 200 Å, with the maximum located around 75 Å (7.5 nm), further supporting the presence of a well-developed mesoporous structure. The structural characteristics of the present Au/γ-Al_2O_3 catalyst are consistent with previously reported Au/γ-Al_2O_3 systems. The catalyst exhibited a BET surface area of 266 m^2 g^{-1} and a mesoporous structure with characteristic dimensions in the range of 7.5–13 nm. These values are comparable to those reported by Cai et al. for commercial γ-Al_2O_3-supported Au catalysts, which exhibited a BET surface area of 240 m^2 g^{-1} and mesopore-size maxima around 5.2 nm. Furthermore, the Au nanoparticles in the present catalyst were previously measured by XRD and HRTEM as 4.2 nm and 3.6 ± 1.4 nm, respectively, which is in close agreement with the highly dispersed Au nanoparticles below 5 nm reported for Au/γ-Al_2O_3 catalysts supported on nanorod γ-Al_2O_3. Cai et al. further demonstrated that improved Au dispersion was associated with enhanced resistance to nanoparticle agglomeration and superior catalytic stability in CO oxidation reactions [32].

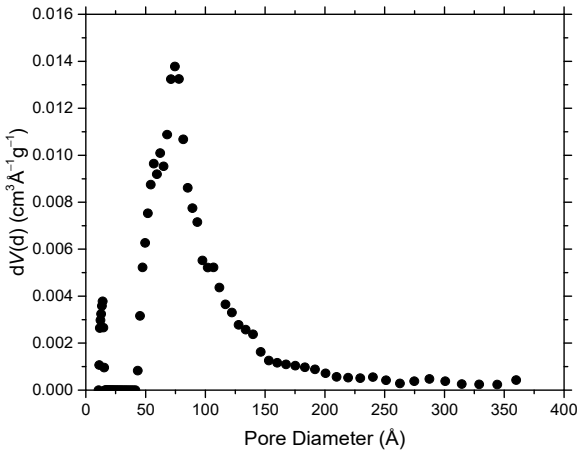


Figure 3. Pore size distribution calculated using the NLDFT method for the Au/γ-Al_2O_3 catalyst. The distribution confirms the presence of nanoscale mesostructural features.

3.2. AFM Surface Morphology

A high-magnification AFM scan is presented in Figure 4. The image reveals nanoscale topographical variations and surface heterogeneity throughout the catalyst surface. Numerous nanoscale depressions, elevations and roughness features can be observed, reflecting the complex morphology generated by the interaction between the gold nanoparticles and the mesoporous alumina support.

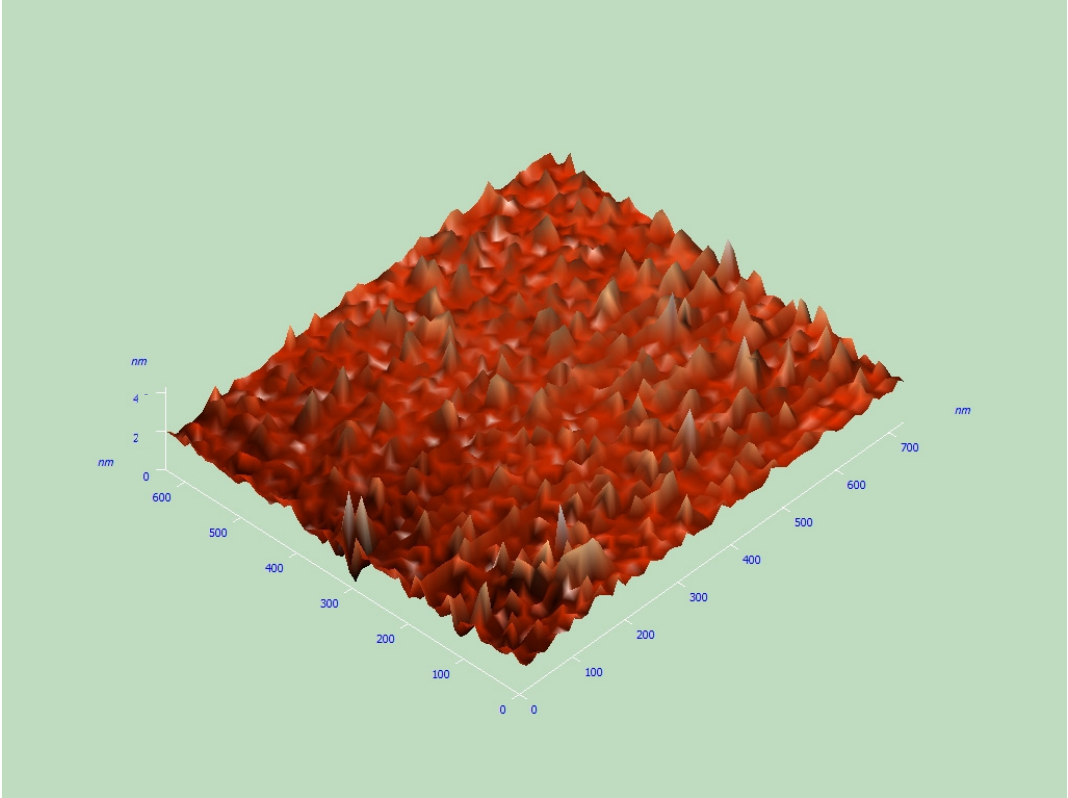


Figure 4. High-resolution AFM topographic image (600 nm × 700 nm) of the Au/γ-Al_2O_3 catalyst. Nanoscale surface heterogeneity, local depressions and elevated regions are observed across the scanned area.

3.3. Quantitative Surface Feature Analysis

To quantify the nanoscale surface morphology, processed AFM images were analysed using threshold segmentation and grain analysis. Rather than interpreting the identified regions as direct measurements of pores, the segmented objects were considered nanoscale surface depressions and topographical features extracted from the AFM height maps. Figure 5 illustrates the threshold-segmented image used for quantitative analysis.

The quantitative grain analysis was performed on the 3 × 3 μm^2 AFM image, corresponding to a total scanned area of 9.0 × 10^6 nm^2. The 600 × 700 nm^2 image was used only for higher-magnification visualization and was not used for the grain-analysis calculations. The AFM image was processed in Gwyddion by image flattening, removal of faulty scan lines where necessary, height-scale adjustment, and noise filtering. Following inversion of the height data, threshold segmentation was performed interactively by adjusting the threshold until individual low-lying regions were visually distinguishable from the surrounding topography without obvious merging of adjacent regions. Quantitative analysis identified 2539 surface depressions within the analysed image, corresponding to a planar surface fraction of 6.71%. The average feature width and length were 22.05 and 7.34 nm, respectively, while the mean characteristic feature size calculated from the grain

analysis was 9.44 nm. The projected area occupied by the segmented surface depressions was 237.8 nm^2. The nanoscale surface depressions identified from the AFM topographic maps and subsequently segmented by grain analysis correspond to the same population of surface features. These depressions were characterized by average maximum and minimum Feret diameters of 22.05 nm and 7.34 nm, respectively, indicating an anisotropic lateral geometry, as shown in Table 2. For comparison purposes, the grain-analysis procedure additionally provided a characteristic feature size of 9.44 nm, which represents a single equivalent-size parameter derived from the projected area of the segmented objects rather than a direct lateral dimension. The projected area corresponds to the two-dimensional area occupied by each surface depression when viewed from above and was used to calculate both the characteristic feature size, through an equivalent circular-area approximation, and the fraction of the scanned surface occupied by the segmented depressions (6.71%). Furthermore, the projected-area distribution provides information on the spatial distribution and morphological heterogeneity of the surface features across the analysed AFM image.

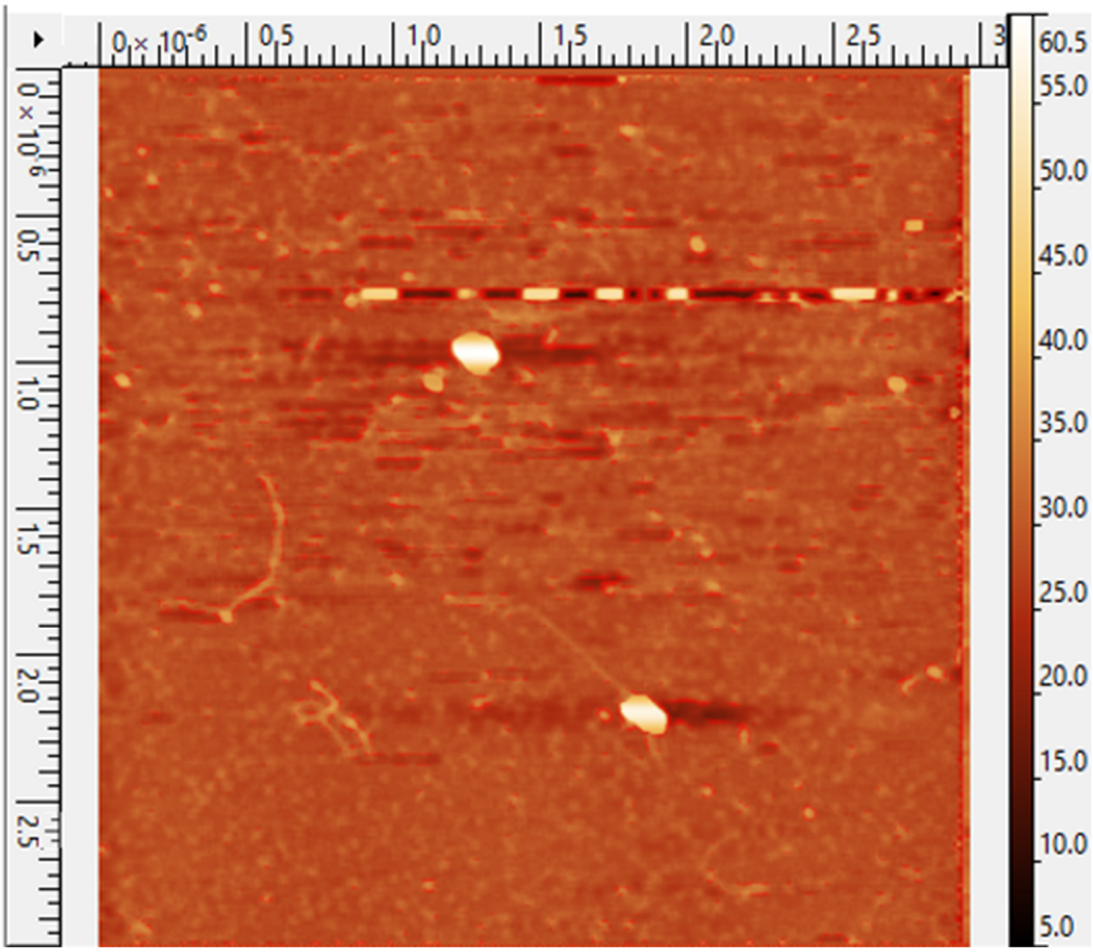


Figure 5. Threshold-segmented AFM image used for quantitative surface-feature analysis. Red regions correspond to nanoscale surface depressions identified through image processing after removal of edge-touching objects and large aggregates.

Table 2. Quantitative analysis of AFM-derived surface depressions.

Parameter	Value
Number of surface depressions	2539
Planar surface fraction (%)	6.71
Feret maximum diameter (nm)	22.05
Feret minimum diameter (nm)	7.34
Mean projected area (nm^2)	237.8

To evaluate the representativeness of the grain-analysis results, selected topographical depressions were independently measured from horizontal and vertical profile lines extracted from the AFM image, as in Figure 6.

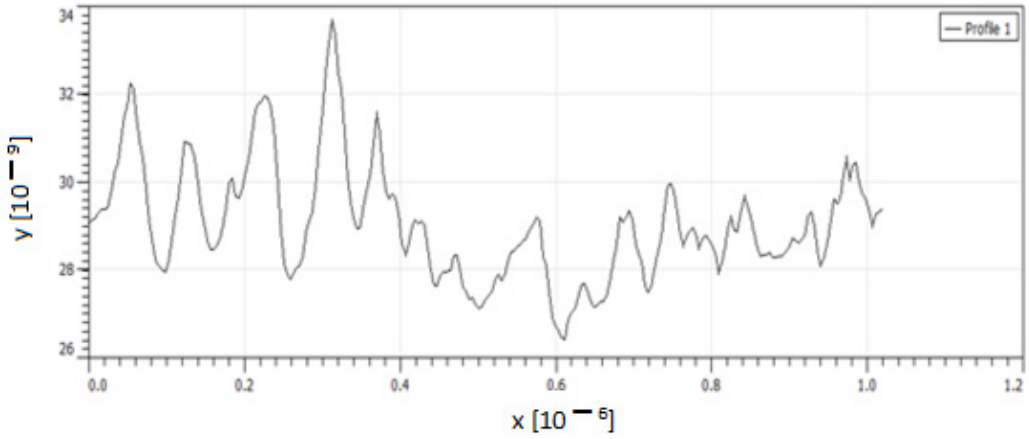


Figure 6. Representative AFM height profile showing a nanoscale surface depression identified along the selected scan line.

The dimensions obtained from manually measured surface depressions were compared with the corresponding dimensions generated by the grain-analysis procedure. Student's *t*-test performed at the 99% confidence level showed that the calculated experimental t-values were smaller than the critical *t*-value for all examined dimensions ($t$crit = 2.567, $\alpha = 0.01$, d$f = 17$). Therefore, the null hypothesis was not rejected, indicating that the differences between the manually measured dimensions and the grain analysis results were statistically insignificant, as shown in Table 3. Consequently, the analysed region was considered representative of the overall set of segmented surface depressions within the AFM image.

Table 3. Statistical validation of AFM measurements using Student's *t*-distribution.

Parameter	Width (nm)	Length (nm)	Characteristic Feature Size (nm)
Mean value	19.23	8.12	12.47
Experimental *t* value	0.92	0.42	1.82

The characteristic dimensions obtained from AFM image analysis (9.4–12.5 nm) are comparable to the dominant mesopore size range identified by nitrogen adsorption measurements (9–13 nm), indicating consistency between the observed surface morphology and the mesostructural characteristics of the catalyst. However, it should be emphasized that AFM provides information only on external surface topography; therefore, the identified depressions should be interpreted as nanoscale surface features rather than direct

measurements of the internal pore network. The characteristic dimensions of the surface depressions fall within the dominant mesopore range determined by nitrogen adsorption (9–13 nm). The AFM tip cannot enter these openings to any significant depth: for an apex radius of 10 nm, the maximum penetration into a 9 nm opening is about 1.1 nm. The depressions are therefore surface openings of the pore network, and their size is compared with the mesopore population as a dimensional correspondence, not as a measurement of internal pore size.

3.4. Surface Roughness Results

Surface roughness was evaluated directly from the AFM topographic maps. Representative roughness profiles are presented in Figures 7–9. The roughness traces reveal significant nanoscale variability arising from the presence of nanoparticles, clusters and larger aggregates distributed on the support surface.

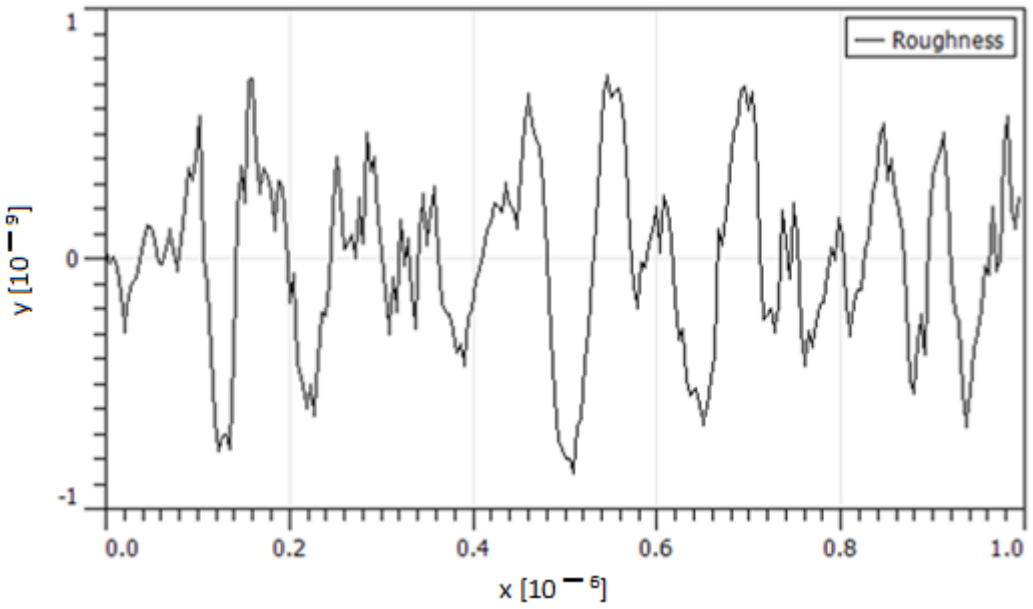


Figure 7. Surface-height profile used for roughness evaluation. The variation in height reflects the nanoscale topographical heterogeneity of the Au/γ-Al_2O_3 catalyst surface.

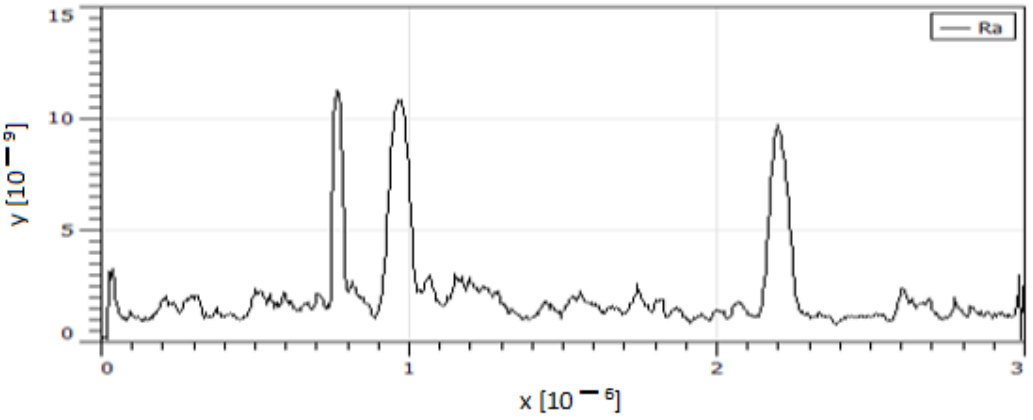


Figure 8. Arithmetic average roughness (*Ra*) distribution calculated from AFM topographic data. The results indicate a moderately rough nanostructured surface.

The arithmetic mean roughness of the surface was determined as:

$$Ra = 2.06 \pm 1.90 \text{ nm}$$

while the root mean square roughness was:

$$Rq = 3.42 \pm 1.91 \text{ nm}$$

The larger *R*q value compared with *R*a reflects the contribution of localized protrusions associated with nanoparticle clusters and aggregates. These results indicate that the catalyst surface exhibits moderate nanoscale roughness and pronounced topographical heterogeneity.

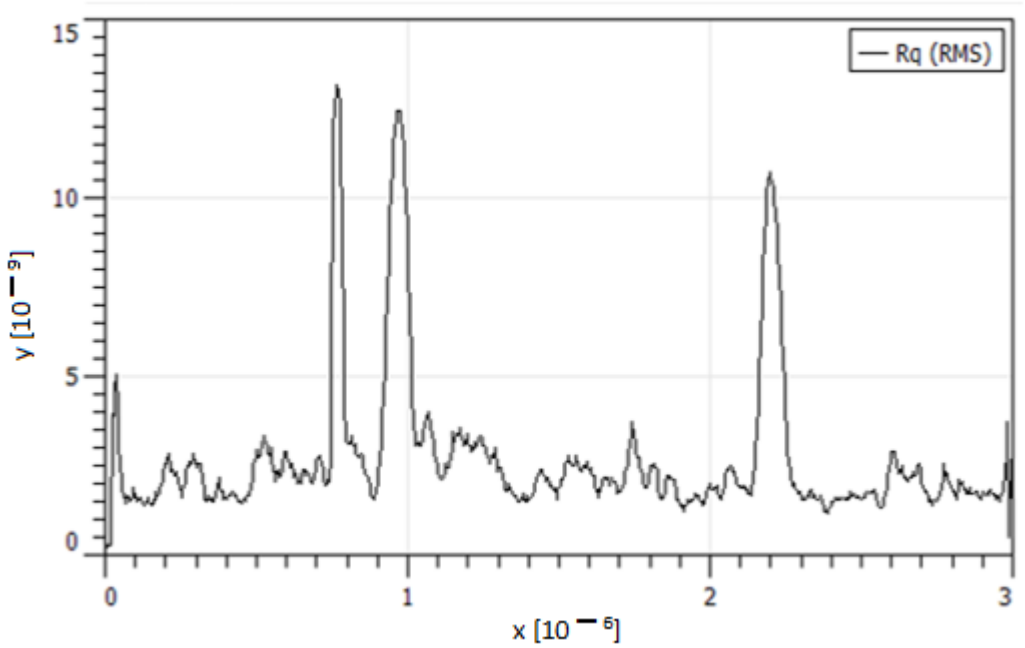


Figure 9. Root mean square roughness (*R*q) distribution obtained from AFM measurements. The higher sensitivity of *R*q to localized height variations highlights the contribution of nanoparticle clusters and aggregates to surface roughness.

4. Discussion

The nitrogen adsorption-desorption measurements demonstrated that the Au/γ-Al_2O_3 catalyst possesses a well-developed mesoporous structure. The Type IV adsorption isotherm with a pronounced hysteresis loop is characteristic of mesoporous materials, while the BET surface area of 266 m^2 g^{-1} and the large total pore volume indicate that γ-Al_2O_3 provides a highly accessible support for the dispersion of gold nanoparticles. The pore size distributions obtained by both BJH and NLDFT analyses confirmed that the dominant structural features of the support fall within the mesoporous range. Specifically, the BJH analysis revealed distribution maxima between approximately 90 and 130 Å, whereas NLDFT analysis yielded a maximum around 75 Å, with both methods indicating pore dimensions characteristic of mesoporous alumina. The pore-size maximum depended on both the calculation method and the isotherm branch, occurring at approximately 13 nm for BJH adsorption, 9 nm for BJH desorption, and 7.5 nm for NLDFT. These values should not be interpreted as independent measurements of a unique pore diameter. BJH analysis is based on the Kelvin equation, an adsorbed-film-thickness correction, and an idealized pore geometry. Moreover, adsorption and desorption represent different pathways of capillary condensation and evaporation. In disordered pore networks, the desorption branch may be influenced by pore blocking and cavitation, shifting the calculated distribution toward smaller apparent diameters. The adsorption-branch maximum of approximately 13 nm is therefore considered the more appropriate BJH descriptor for the present material, whereas the 9 nm desorption maximum is interpreted cautiously as an evaporation- and network-dependent value.

NLDFT returned a lower maximum of approximately 7.5 nm because it models adsorption and fluid-density variations within idealized pores at the molecular level rather than applying the macroscopic Kelvin equation. Nevertheless, none of the calculated maxima is treated as an absolute geometric pore diameter in the absence of independent structural validation. Collectively, the analyses consistently establish that the catalyst is mesoporous, while indicating that its modal pore dimension is method-dependent and lies approximately between 7.5 and 13 nm.

The high surface area and mesoporosity of γ-Al_2O_3 are important for supported gold catalysts because they promote the dispersion of the active phase and facilitate access of reactants to active sites. The predominance of external surface area (255 m^2 g^{-1}) and the negligible micropore contribution indicate that most of the catalytic surface is readily accessible, which is beneficial for catalytic processes involving gas-phase reactants.

Depressions may in principle arise from pore mouths, interparticle voids, grain boundaries or tip artefacts. The H3 hysteresis indicates slit-like mesopores between plate-like γ-Al_2O_3 particles. For this support, the openings of these voids at the external surface are the interparticle gaps, so pore mouths and interparticle voids are the same objects. Tip convolution narrows depressions, so after blind tip reconstruction, the measured widths are lower bounds on the true opening size. Same-region SEM–AFM or FIB-SEM would provide direct confirmation and is planned for future work.

AFM characterization provided complementary information that cannot be obtained directly from nitrogen porosimetry. While adsorption measurements describe the internal porous architecture, AFM enabled direct visualization of the external surface morphology at the nanoscale.

A high-magnification AFM image highlighted the complex nanoscale topography of the catalyst surface. Numerous protrusions and depressions were observed across the scanned region, reflecting the interaction between the porous alumina support and the deposited gold nanoparticles. Such surface heterogeneity may influence the distribution of adsorption sites and contribute to variations in local surface reactivity.

A major objective of this work was to evaluate whether quantitative AFM image analysis could provide information related to the structural characteristics independently determined by nitrogen adsorption. Following threshold segmentation and grain analysis, 2539 nanoscale surface depressions were identified within the analysed area. It is important to emphasize again that these segmented objects should not be interpreted as direct measurements of bulk pores but rather as the mouths of surface pores. AFM probes only the external surface topography, whereas porosimetry characterizes the internal pore network. Consequently, the detected objects are more appropriately described as surface depressions or topographical features that may be associated with openings or manifestations of the underlying mesostructure.

The mean characteristic feature size determined by grain analysis was 9.44 nm, while independent statistical analysis yielded a value of 12.47 nm. The reported characteristic feature size of 9.44 nm is not a direct AFM measurement but a statistical parameter derived from image processing and grain analysis of the segmented AFM topography. These dimensions are remarkably close to the dominant mesopore size range identified by BJH analysis (9–13 nm). The agreement does not demonstrate that AFM directly measures pore size; however, it suggests that the observed surface topography reflects structural characteristics associated with the mesoporous alumina support.

The statistical validation performed using Student's *t*-distribution demonstrated good agreement between local measurements extracted from selected line profiles and the image-wide grain analysis results. In all examined cases, the experimental *t*-values remained below the critical value, indicating that the differences between local and global

measurements were statistically insignificant. Therefore, the analysed AFM region can be considered representative of the overall scanned surface. The present AFM analysis is based on a representative scan area and therefore provides information on the local surface morphology of the catalyst. Additional measurements acquired from multiple randomly selected surface regions and independent catalyst samples would be beneficial for establishing statistical variability and assessing the broader representativeness of the observed surface-feature distributions.

Surface roughness analysis revealed arithmetic and root mean square roughness values of $Ra = 2.06 \pm 1.90$ nm and $Rq = 3.42 \pm 1.91$ nm, respectively. The higher Rq value reflects the contribution of isolated peaks associated with nanoparticle clusters and aggregates. These roughness values indicate a moderately rough nanostructured surface and confirm the heterogeneous character of the Au/γ-Al_2O_3 catalyst. The statistical analysis demonstrated that local measurements obtained from representative AFM profiles were in good agreement with image-wide grain analysis results, supporting the reliability of the image-processing methodology. Surface roughness parameters of $Ra = 2.06 \pm 1.90$ nm and $Rq = 3.42 \pm 1.91$ nm confirmed the presence of a moderately rough and heterogeneous nanostructured surface. The higher value of Rq compared with Ra reflects the increased sensitivity of the root mean square roughness to infrequent but pronounced height variations on the surface. The ratio $Rq/Ra = 1.66$ is considerably larger than the value of approximately 1.25 expected for an ideal Gaussian height distribution, indicating that the surface contains sparse topographical outliers in the form of localized protrusions or aggregates rather than exhibiting purely random roughness. This observation is consistent with the AFM images, which reveal the presence of protrusions compatible with Au nanoparticles and their aggregates distributed across the γ-Al_2O_3 support. The roughness parameters therefore suggest a moderately rough surface with significant topographical heterogeneity and a non-Gaussian height distribution. The arithmetic average surface roughness (Ra) distribution was calculated from the AFM height map. The error bars represent the standard deviation of the surface height distribution determined by Gwyddion. The reported $\pm$ values do not represent experimental uncertainties or variability between independent AFM scans. Instead, they correspond to the standard deviation of the surface height distribution calculated by Gwyddion from the analysed AFM topographic map. Consequently, the relatively large values reflect the broad range of surface heights present within the scanned area rather than poor measurement precision.

Overall, the results demonstrate that nitrogen adsorption and AFM provide complementary structural information. Nitrogen porosimetry quantitatively characterizes the internal porous architecture, whereas AFM provides direct information on external surface morphology, roughness, nanoparticle distribution and nanoscale surface heterogeneity. The combined application of both techniques therefore offers a more comprehensive description of catalyst structure than either method alone. Future work may benefit from the analysis of multiple AFM scan locations, the application of tip-convolution corrections, and the correlation of surface topography with catalytic performance and adsorption behavior. The catalytic performance and stability of Au/γ-Al_2O_3 catalysts are strongly influenced by the combined effects of support texture, surface morphology, and gold nanoparticle dispersion. The present catalyst exhibited a high BET surface area (266 m^2 g^{-1}) and a well-developed mesoporous structure. Such mesoporous frameworks are known to promote the dispersion of supported Au nanoparticles and facilitate access of reactants to catalytically active sites. The AFM analysis further revealed a heterogeneous surface morphology, indicating the presence of a structurally diverse catalytic surface. The average Au particle size previously determined by HRTEM (3.6 ± 1.4 nm) and XRD (4.2 nm) suggests a highly dispersed gold phase, which is generally associated with enhanced catalytic activity in CO oxidation and

related reactions due to the increased density of exposed active sites. Previous studies have demonstrated that Au nanoparticles smaller than approximately 5 nm exhibit superior catalytic activity compared with larger particles, while improved dispersion and stronger metal-support interactions can significantly enhance resistance to nanoparticle agglomeration and thermal deactivation [32]. Therefore, the combination of high surface area, mesoporosity, and nanoscale Au dispersion observed in the present catalyst is expected to favor both catalytic activity and long-term stability.

5. Conclusions

A 5 wt.% Au/γ-Al_2O_3 catalyst was characterized using a combination of nitrogen adsorption-desorption porosimetry and Atomic Force Microscopy in order to investigate both its textural properties and surface morphology. Nitrogen adsorption measurements revealed a Type IV isotherm and confirmed the mesoporous nature of the catalyst. The material exhibited a BET specific surface area of 266 m^2 g^{-1}, a total pore volume of 0.928 cm^3 g^{-1}, and dominant pore-size distributions centered between approximately 9 and 13 nm.

AFM imaging showed that the catalyst surface is highly heterogeneous and consists of protrusions compatible with Au nanoparticles and their aggregates distributed across the γ-Al_2O_3 support. Quantitative image analysis identified 2539 nanoscale surface depressions within the investigated area, corresponding to a planar surface fraction of 6.71%. The characteristic dimensions of these surface features ranged between approximately 9 and 12 nm and were found to be consistent with the mesoporous dimensions obtained independently from nitrogen adsorption measurements.

The combined methodology employed in this work provides a comprehensive description of the structural and topographical characteristics of Au/γ-Al_2O_3 catalysts and may be useful for future studies seeking to relate catalyst morphology to adsorption and catalytic performance. Although AFM cannot directly characterize the internal pore network, the observed correspondence between AFM-derived surface features and porosimetric measurements suggests that nanoscale surface morphology may reflect important aspects of the underlying mesostructure. Once a correlation of bulk pore and surface feature dimensions is established for a particular type of catalyst, via both porosimetry and AFM preliminary experiments respectively, then AFM can be used for further routine tests to infer catalyst porosity. Because AFM does not directly probe the internal pore network, AFM-derived surface depressions should not be interpreted as direct measurements of internal mesopores. The similarity between selected dimensional ranges obtained by the two techniques is therefore treated as an observation requiring further correlative validation, rather than as evidence of equivalence. Future studies combining replicate AFM imaging with electron microscopy or other three-dimensional structural methods may help determine whether specific surface-topography descriptors are systematically related to bulk textural properties. AFM should nevertheless be regarded as complementary to, and not a replacement for, nitrogen adsorption porosimetry.

Author Contributions: Conceptualization, D.G. and D.-P.T.; methodology, C.P.; software, D.-P.T.; validation, D.G., and S.S.; formal analysis, D.-P.T.; investigation, D.-P.T.; writing—original draft preparation, D.-P.T.; writing—review and editing, D.G.; visualization, D.-P.T.; supervision, D.G.; project administration, D.G. All authors have read and agreed to the published version of the manuscript.

Funding: This research was funded by the Research committee of Aristotle University of Thessaloniki (Action A: project 91522).

Data Availability Statement: The data presented in this study are available on request from the corresponding author.

Acknowledgments: During the preparation of this manuscript, the authors used Claude AI, Sonnet 5.5 for the purposes of text editing. The authors have reviewed and edited the output and take full responsibility for the content of this publication.

Conflicts of Interest: The authors declare no conflict of interest.

Abbreviations

The following abbreviations are used in this manuscript:

AFM	Atomic Force Microscopy
AAS	Atomic Absorption Spectroscopy
BET	Brunauer–Emmett–Teller
BJH	Barrett–Joyner–Halenda
CSG	Contact Silicon Group (AFM cantilever series designation)
HRTEM	High-Resolution Transmission Electron Microscopy
MES	Mössbauer Emission Spectroscopy
NLDFT	Non-Local Density Functional Theory
PSD	Pore Size Distribution
Ra	Arithmetic Average Roughness
Rq	Root Mean Square Roughness
RMS	Root Mean Square
XPS	X-Ray Photoelectron Spectroscopy
XRD	X-Ray Diffraction

References

1. Somorjai, G.A.; Li, Y. *Introduction to Surface Chemistry and Catalysis*; Wiley: Hoboken, NJ, USA, 2010.
2. Stiles, A.B. *Catalyst Supports and Supported Catalysts: Theoretical and Applied Concepts*; Butterworths Scientific Ltd.: Guildford, UK, 1987.
3. Tanabe, K.; Hölderich, W.F. Industrial application of solid acid-base catalysts. *Appl. Catal. A Gen.* **1999**, *181*, 399–434. [CrossRef]
4. Argyle, M.D.; Bartholomew, C.H. Heterogeneous catalyst deactivation and regeneration: A review. *Catalysts* **2015**, *5*, 145–269. [CrossRef]
5. Papadopoulou, C.; Matralis, H.; Verykios, X. Utilization of biogas as a renewable carbon source: Dry reforming of methane. In *Catalysis for Alternative Energy Generation*; Guczi, L., Erdőhelyi, A., Eds.; Springer: New York, NY, USA, 2012; pp. 57–127.
6. Zhou, R.-S.; Snyder, R.L. Structures and transformation mechanisms of the η, γ and θ transition aluminas. *Acta Crystallogr. B* **1991**, *47*, 617–630. [CrossRef]
7. Stuart, N.M.; Sohlberg, K. The microstructure of γ-alumina. *Energies* **2021**, *14*, 6472. [CrossRef]
8. Digne, M.; Sautet, P.; Raybaud, P.; Euzen, P.; Toulhoat, H. Use of DFT to achieve a rational understanding of acid-base properties of γ-alumina surfaces. *J. Catal.* **2004**, *226*, 54–68. [CrossRef]
9. Prins, R. On the structure of γ-Al_2O_3. *J. Catal.* **2020**, *392*, 336–346. [CrossRef]
10. Pinto, H.P.; Nieminen, R.M.; Elliott, S.D. Ab initio study of γ-Al_2O_3 surfaces. *Phys. Rev. B* **2004**, *70*, 125402. [CrossRef]
11. Braulio, M.A.L.; Rigaud, M.; Buhr, A.; Parr, C.; Pandolfelli, V.C. Spinel-containing alumina-based refractory castables. *Ceram. Int.* **2011**, *37*, 1705–1724. [CrossRef]
12. Brunauer, S.; Emmett, P.H.; Teller, E. Adsorption of gases in multimolecular layers. *J. Am. Chem. Soc.* **1938**, *60*, 309–319. [CrossRef]
13. Bardestani, R.; Patience, G.S.; Kaliaguine, S. Experimental methods in chemical engineering: Specific surface area and pore size distribution measurements: BET, BJH, and DFT. *Can. J. Chem. Eng.* **2019**, *97*, 2781–2791. [CrossRef]
14. Sing, K.S.W. The use of nitrogen adsorption for the characterisation of porous materials. *Colloids Surf. A* **2001**, *187–188*, 3–9. [CrossRef]
15. Lecloux, A. The use of adsorption methods for the assessment of the surface area and pore size distribution of heterogeneous catalysts. *Stud. Surf. Sci. Catal.* **1993**, *79*, 419–438. [CrossRef]
16. Haugstad, G. *Atomic Force Microscopy: Understanding Basic Modes and Advanced Applications*; Wiley: Hoboken, NJ, USA, 2012.
17. West, P.E. *Introduction to Atomic Force Microscopy: Theory, Practice, Applications*; Pacific Nanotechnology: Santa Clara, CA, USA, 2007.
18. Wilson, R.A.; Bullen, H.A. *Introduction to Scanning Probe Microscopy (SPM): Basic Theory Atomic Force Microscopy (AFM)*; Northern Kentucky University: Highland Heights, KY, USA, 2006.
19. Do, V.-H.; Lee, J.-M. Surface engineering for stable electrocatalysis. *Chem. Soc. Rev.* **2024**, *53*, 2693–2737. [CrossRef] [PubMed]

20. Gavriil, D.; Georgaka, A.; Loukopoulos, V.; Karaiskakis, G.; Nieuwenhuys, B.E. On the mechanism of selective CO oxidation on nanosized Au/γ-Al_2O_3 catalysts. *Gold Bull.* **2006**, *39*, 159–165. [CrossRef]
21. Loukopoulos, V.; Gavriil, D.; Karaiskakis, G.; Georgaka, A. Gas chromatographic investigation of the effects of hydrogen and temperature on the nature of the active sites related to CO adsorption on nanosized Au/γ-Al_2O_3. *J. Chromatogr. A* **2007**, *1157*, 465–472. [CrossRef] [PubMed]
22. Gavriil, D.; Georgaka, A.; Loukopoulos, V.; Karaiskakis, G.; Nieuwenhuys, B.E. H_2 and CO_2 coadsorption effects in CO adsorption over nanosized Au/γ-Al_2O_3 catalysts. *J. Chromatogr. A* **2008**, *1187*, 224–230. [CrossRef] [PubMed]
23. Gavriil, D.; Georgaka, A.; Karaiskakis, G. Kinetic study of oxygen adsorption over nanosized Au/γ-Al_2O_3 supported catalysts under selective CO oxidation conditions. *Molecules* **2012**, *17*, 4878–4895. [CrossRef] [PubMed]
24. Gavriil, D. CO oxidation on nanosized Au/Al_2O_3 by surface hydroxyl groups and in the absence of O_2, studied by inverse gas chromatography. *Catal. Today* **2015**, *249*, 62–68. [CrossRef]
25. Grisel, R.J.H. Supported Gold Catalysts for Environmental Applications. Ph.D. Thesis, Leiden University, Leiden, The Netherlands, 2002.
26. Grisel, R.J.H.; Nieuwenhuys, B.E. Selective Oxidation of CO, over Supported Au Catalysts. *J. Catal.* **2001**, *199*, 48–59. [CrossRef]
27. Barrett, E.P.; Joyner, L.G.; Halenda, P.P. The determination of pore volume and area distributions in porous substances. I. Computations from nitrogen isotherms. *J. Am. Chem. Soc.* **1951**, *73*, 373–380. [CrossRef]
28. Kupgan, G.; Liyana-Arachchi, T.P.; Colina, C.M. NLDFT pore size distribution in amorphous microporous materials. *Langmuir* **2017**, *33*, 11138–11145. [CrossRef] [PubMed]
29. Jiao, K.; Yao, S.; Zhang, K.; Hu, W.; Cao, J. The evolution of nanopores and surface roughness in naturally matured coals in South China: An atomic force microscopy and image processing study. *Fuel* **2018**, *234*, 1123–1131. [CrossRef]
30. Liu, Y.; Zhang, J.; Li, X.; Wang, Z. Quantitative analysis of coal nanopore characteristics using atomic force microscopy. *Powder Technol.* **2019**, *346*, 332–340. [CrossRef]
31. Barbosa, A.; Borges, J.; Meira, D.I.; Costa, D.; Rodrigues, M.S.; Rebelo, R.; Correlo, V.M.; Vaz, F.; Reis, R.L. Development of label-free plasmonic Au-TiO_2 thin film immunosensor devices. *Mater. Sci. Eng. C* **2019**, *100*, 424–432. [CrossRef] [PubMed]
32. Cai, W.; Sun, X.; Bao, Y.; Guo, J.; Liu, A.; Hu, K.; Feng, L. Distinct Morphology-Dependent Behaviors for Au/γ-Al_2O_3 Catalysts: Enhanced Thermal Stabilization in CO Oxidation Reaction. *RSC Adv.* **2023**, *13*, 9010–9019. [CrossRef] [PubMed]

Disclaimer/Publisher's Note: The statements, opinions and data contained in all publications are solely those of the individual author(s) and contributor(s) and not of MDPI and/or the editor(s). MDPI and/or the editor(s) disclaim responsibility for any injury to people or property resulting from any ideas, methods, instructions or products referred to in the content.